

Laser parameters affecting the asymmetric radiation of the electron in tightly focused intense laser pulses

Xing-Yu Li(李星宇), Wan-Yu Xia(夏婉瑜), You-Wei Tian(田友伟), and Shan-Ling Ren(任山令)
Citation: Chin. Phys. B, 2023, 32 (**12**): 124205. DOI: 10.1088/1674-1056/acd3dd
Journal homepage: http://cpb.iphy.ac.cn; http://iopscience.iop.org/cpb

What follows is a list of articles you may be interested in

High-speed directly modulated distributed feedback laser based on detuned loading and photon-photon resonance effect

Yun-Shan Zhang(张云山), Yi-Fan Xu(徐逸帆), Ji-Lin Zheng(郑吉林), Lian-Yan Li(李连艳), Tao Fang(方涛), and Xiang-Fei Chen(陈向飞)
Chin. Phys. B, 2023, 32 (**9**): 094204. DOI: 10.1088/1674-1056/acc8c1

Single-frequency linearly polarized *Q*-switched fiber laser based on Nb_2GeTe_4 saturable absorber

Si-Yu Chen(陈思雨), Hai-Qin Deng(邓海芹), Wan-Ru Zhang(张万儒), Yong-Ping Dai(戴永平), Tao Wang(王涛), Qiang Yu(俞强), Can Li(李灿), Man Jiang(姜曼), Rong-Tao Su(粟荣涛), Jian Wu(吴坚), and Pu Zhou(周朴)
Chin. Phys. B, 2023, 32 (**7**): 074203. DOI: 10.1088/1674-1056/acad6d

Analysis of CV mode selected resonator based on vectorial eigenvector method

You-You Hu(胡友友), Jian-Tai Dou(窦健泰), Bo-Wei Luo(罗博伟), Chang-Yu He(贺昌玉)
Chin. Phys. B, 2019, 28 (**2**): 024210. DOI: 10.1088/1674-1056/28/2/024210

Dynamical properties of total intensity fluctuation spectrum in two-mode Nd:YVO_4 microchip laser

Zhang Shao-Hui (张韶辉), Zhang Shu-Lian (张书练), Tan Yi-Dong (谈宜东), Sun Li-Qun (孙利群)
Chin. Phys. B, 2015, 24 (**12**): 124203. DOI: 10.1088/1674-1056/24/12/124203

1.12-W Q-switched Yb:KGW laser based on transmission-type Bi_2Se_3 saturable absorber

Liu Jing-Hui (刘京徽), Tian Jin-Rong (田金荣), Hu Meng-Ting (胡梦婷), Xu Run-Qin (徐润亲), Dou Zhi-Yuan (窦志远), Yu Zhen-Hua (于振华), Song Yan-Rong (宋晏蓉)
Chin. Phys. B, 2015, 24 (**2**): 024215. DOI: 10.1088/1674-1056/24/2/024215

Laser parameters affecting the asymmetric radiation of the electron in tightly focused intense laser pulses

Xing-Yu Li(李星宇)[1], Wan-Yu Xia(夏婉瑜)[2], You-Wei Tian(田友伟)[3,†], and Shan-Ling Ren(任山令)[3]

[1] *Bell Honors School, Nanjing University of Posts and Telecommunications, Nanjing* 210023, *China*
[2] *College of Management, Nanjing University of Posts and Telecommunications, Nanjing* 210023, *China*
[3] *College of Science, Nanjing University of Posts and Telecommunications, Nanjing* 210023, *China*

(Received 18 December 2022; revised manuscript received 13 April 2023; accepted manuscript online 10 May 2023)

The nonlinear radiation of the electron is a distinctive feature of the action of tightly focused linearly polarized lasers. In this paper, from the perspective of radiation symmetry, the effect of laser parameters on the electron radiation power in the time domain is studied systematically. An asymmetric bimodal structure is found in the time domain in the direction of the maximum radiation. For this special structure, an explanation is given based on the electron dynamics perspective. The structure is compared with the symmetric bimodal structure in the classical theory. The increase in laser intensity, while significantly increasing the radiated power of the electron, exacerbates the asymmetry of the electron radiation. The variation in the initial phase of the laser leads to a periodic variation in the electron motion, which results in a periodic extension of the electron spatial radiation with a period of π. Moreover, the existence of jump points with a phase difference of π in the range of 0–2π is found. The increase in pulse width reduces the radiated power, extends the radiation range, and alleviates the radiation asymmetry. The results in this paper contribute to the study of electron radiation characteristics in intense laser fields.

Keywords: laser optics, nonlinear Thomson scattering, tightly focused laser, asymmetric radiation

PACS: 42.55.–f, 41.60.Cr, 42.65.–k, 42.50.Hz **DOI:** 10.1088/1674-1056/acd3dd

1. Introduction

As an approximation of Compton scattering in the low-energy region,[1] Thomson scattering refers to the elastic scattering process between a free-charged particle and an electromagnetic field. In the 1980s, Mourou *et al.*[2] proposed the chirped pulse amplification (CPA) technique, which greatly improved the quality of laser pulses. The CPA technique is able to compress the width of the laser pulse and increase the peak power.[3–5] After proper focusing, a laser with relativistic light intensity can be obtained.[6,7] This great progress has triggered a rethinking of Thomson scattering. Under the action of a laser of relativistic light intensity, the oscillation speed of the electron approaches the speed of light.[8] The effect of the magnetic field on the electron has been greatly enhanced and is already comparable to the electric field, which leads to the nonlinear oscillatory motion of the electron. As a result, Thomson scattering becomes a nonlinear problem, namely, nonlinear Thomson scattering (NTS). High-energy rays (e.g., x-rays) produced using NTS have many applications in medical diagnostics,[9,10] nuclear physics,[11,12] and other fields.[13,14]

A number of theoretical and experimental studies have been conducted to discuss the radiation properties of the electron under the action of the laser pulse.[15–17] From the perspective of the spatial domain, Lee *et al.*[18] numerically simulated the spatial characteristics of Thomson scattering from stationary single electron under the action of intense lasers with different polarization states. Chang *et al.*[19] discussed the collimation of electron radiation using tightly focused circularly polarized laser pulses colliding with an ultrahigh energy electron. From the perspective of the frequency domain, POPA *et al.*[20] gave an exact calculation of Thomson scattering higher harmonics. Hartemann *et al.*[21] proposed that the use of circularly polarized laser pulses with a planar envelope could effectively improve the monochromatic nature of the electron radiation. However, most of the existing studies focus on the spatial and frequency domains, while ignoring the radiation phenomenon of the electron in the time domain. Today, Cao *et al.*[22] exploited the nonlinear Thomson scattering to achieve a single attosecond pulse. Lü *et al.*[23] used tightly focused laser pulses to interact with the electron and found the phenomenon of asymmetric radiation of the electron. However, the study by Lü *et al.* was limited to laser pulses with specific parameters and ignored the discussion in the general case.

To solve the above problems, the effects of various parameters on electron radiation under the action of a tightly focused linearly polarized laser pulse are comprehensively studied. The results show that although the increase in laser intensity can significantly increase the maximum radiated power, it exacerbates the asymmetry of electron radiation. On the contrary, the increase in the pulse width reduces the maximum radiated power and alleviates the asymmetry of the electron

†Corresponding author. E-mail: tianyw@njupt.edu.cn

© 2023 Chinese Physical Society and IOP Publishing Ltd

radiation. In addition, the increase in the pulse width expands the radiation range. With the variation in the initial phase, we also find a periodic variation in the electron asymmetric radiation with a period of π. In the range of 0–2π, there exist jump points with the phase difference of π. Considering the above phenomenon, reasonable explanations are given based on electrodynamics.

The rest of the paper is organized as follows. In Section 2, based on electrodynamic principles, expressions for the electromagnetic field of laser, equation of motion of the electron, and the electron radiation (i.e., NTS radiation) are derived. In Section 3, the effects of laser intensity, initial phase, and pulse width on the electron radiation are analyzed. From the perspective of the time domain, we focus on the characteristics of electron asymmetric radiation. In Section 4, the effects of laser parameters on the electron asymmetric radiation are summarized. In addition, the prospects of the application of this research are presented.

2. Theory and formula

This paper is based on a single-electron model for numerical simulation, which has the advantage of high accuracy and high speed. The model is beneficial to improve the safety and effectiveness of detecting laser parameters.

In the numerical simulation, the electron is set at the coordinate origin. The electron interacts with a Gaussian tightly focused linearly polarized laser pulse. The pulse propagates in the $+z$ direction, as shown in Fig. 1.

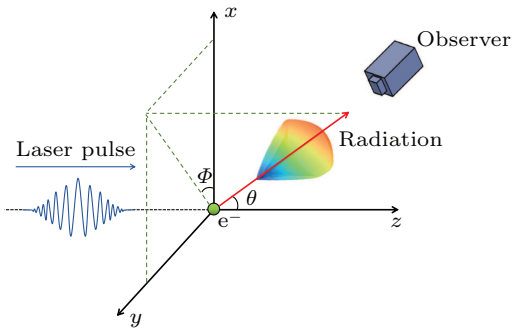


Fig. 1. Diagram of a tightly focused linearly polarized laser pulse interacting with a stationary electron.

Based on the single-electron model, the rest mass of the electron $m = 9.11 \times 10^{-31}$ kg, and the charge of the electron $e = 1.6 \times 10^{-19}$ C. Meanwhile, the wavelength of the laser pulse $\lambda_0 = 1$ μm and the wave number $k_0 = 2\pi/\lambda_0$. The laser frequency is ω_0. The laser amplitude is a_0, which is a dimensionless physical quantity. The laser intensity is I in W·cm^{-2}. Note that $a_0 = 0.85 \times 10^{-9}\sqrt{I\lambda_0^2}$.

In the next sections, the spatial and temporal coordinates in each equation have been normalized by k_0^{-1} and ω_0^{-1}.

2.1. Laser pulses

As mentioned in Section 1, the intensity of the laser pulse can reach the level of relativistic light intensity after focusing on a small dimension. Therefore, a detailed study of the laser electric and magnetic fields near the beam focus is required.[24] However, the field description based on low-order Gaussian beams is not precise enough. Some scholars adopted the near-axis approximation treatment to reduce the computational effort of numerical simulation.[17,19] The method ignored the effect of the longitudinal field, which led to a high error between the simulation results and the actual situation.[17] In contrast, the description of the laser electric and magnetic fields using higher-order field effects is more accurate.

The laser beam shown in Fig. 1 is modeled by a linearly polarized vector potential along the $+x$ axis. Based on the higher-order field effects of the laser electric field, the three components of $\boldsymbol{E}$ can be expressed as[24,26]

$$\begin{aligned} E_x &= E_L\Big\{S_0+\varepsilon^2\left[\xi^2 S_2-\frac{\rho^4 S_3}{4}\right] \\ &\quad+\varepsilon^4\left[\frac{S_2}{8}-\frac{\rho^2 S_3}{4}-\frac{\rho^2\left(\rho^2-16\xi^2\right)S_4}{16}\right. \\ &\quad\left.-\frac{\rho^4\left(\rho^2+2\xi^2\right)S_5}{8}+\frac{\rho^8 S_6}{32}\right]\Big\}, \end{aligned} \tag{1}$$

$$E_y = E_L\xi\kappa\left\{\varepsilon^2 S_2+\varepsilon^4\left[\rho^2 S_4-\frac{\rho^4 S_5}{4}\right]\right\}, \tag{2}$$

$$\begin{aligned} E_z &= E_L\xi\Big\{\varepsilon C_1+\varepsilon^3\left[-\frac{C_2}{2}+\rho^2 C_3-\frac{\rho^4 C_4}{4}\right] \\ &\quad+\varepsilon^5\left[-\frac{3C_3}{8}-\frac{3\rho^2 C_4}{8}+\frac{17\rho^4 C_5}{16}\right. \\ &\quad\left.-\frac{3\rho^6 C_6}{8}+\frac{\rho^8 C_7}{32}\right]\Big\}. \end{aligned} \tag{3}$$

Similarly, the magnetic field component of a laser pulse can be described as[24,26]

$$B_x = 0, \tag{4}$$

$$\begin{aligned} B_y &= E_L\Big\{S_0+\varepsilon^2\left[\frac{\rho^2 S_2}{2}-\frac{\rho^4 S_3}{4}\right] \\ &\quad+\varepsilon^4\left[-\frac{S_2}{8}+\frac{\rho^2 S_3}{4}+\frac{5\rho^4 S_4}{16}-\frac{\rho^6 S_5}{4}+\frac{\rho^8 S_6}{32}\right]\Big\}, \end{aligned} \tag{5}$$

$$\begin{aligned} B_z &= E_L\kappa\Big\{\varepsilon C_1+\varepsilon^3\left[\frac{C_2}{2}+\frac{\rho^2 C_3}{2}-\frac{\rho^4 C_4}{4}\right] \\ &\quad+\varepsilon^5\left[\frac{3C_3}{8}+\frac{3\rho^2 C_4}{8}+\frac{3\rho^4 C_5}{16}-\frac{\rho^6 C_6}{4}+\frac{\rho^8 C_7}{32}\right]\Big\}, \end{aligned} \tag{6}$$

where $\xi = x/w_0$, $\kappa = y/w_0$, $r^2 = x^2+y^2$, and $\rho = r/w_0$. $\varepsilon = w_0/z_R$ is the diffraction angle, which is capable of measuring the divergence of the beam. In tightly focused intense laser pulses, the ε^5 term contributes to ensure the accuracy of describing the electromagnetic field. w_0 is the waist radius.

The cross section through the z-axis at any point is also circular with a radius of $w = w_0\sqrt{1+(z/z_{\rm R})^2}$. $z_{\rm R} = \pi w_0^2/\lambda_0$ is the Rayleigh length.

The remaining physical quantities in Eqs. (1)–(6) can be expressed as[25]

$$E_L = E_0 \frac{w_0}{w} \mathrm{e}^{-\frac{\eta^2}{L^2}-\frac{r^2}{w^2}}, \tag{7}$$

$$s_n = \left(\frac{w_0}{w}\right)^n \sin(\varphi + n\varphi_{\rm G}), \quad n = 0,1,2,\ldots, \tag{8}$$

$$C_n = \left(\frac{w_0}{w}\right)^n \cos(\varphi + n\varphi_{\rm G}), \quad n = 0,1,2,\ldots, \tag{9}$$

$$\boldsymbol{E} = -\frac{1}{c}\frac{\partial \boldsymbol{A}}{\partial t}, \quad \boldsymbol{B} = \nabla \times \boldsymbol{A}, \tag{10}$$

where $E_0 = a_0\omega_0 mc/e$ is the electric field amplitude. c is the speed of light, and $c = 3\times10^8\ \mathrm{m\cdot s^{-1}}$. $\eta = \omega_0 t - k_0 z$. L is the pulse width, i.e., half height full width. The phase $\varphi = \varphi_{\rm P} + \varphi_{\rm G} - \varphi_R + \varphi_0$. $\varphi_{\rm P}$ is the plane wave phase. $\varphi_{\rm G} = \tan^{-1} z/z_{\rm f}$ is the Gooey phase related to the Rayleigh length. $\varphi_R = \omega_0(x^2+y^2)/(2cR)$ is the phase relevant to the wavefront curvature. $R(z) = z(1+z_{\rm R}^2/z^2)$ is the radius of curvature before the pulsed laser. φ_0 is the initial phase, which is determined by the laser. It is worth noting that the fields given should satisfy Maxwell's equation $\nabla\cdot\boldsymbol{E} = \nabla\cdot\boldsymbol{B} = 0$.

2.2. Motion of electron

Under the action of a tightly focused intense laser pulse, the equation of motion of electron can be determined by the Lorentz equation and the energy equation[25]

$$\frac{\mathrm{d}\boldsymbol{p}}{\mathrm{d}t} = -e[\boldsymbol{E} + \boldsymbol{u}\times\boldsymbol{B}], \tag{11}$$

$$\frac{\mathrm{d}W}{\mathrm{d}t} = -ec\boldsymbol{u}\cdot\boldsymbol{E}, \tag{12}$$

where $\boldsymbol{p} = \gamma mc\boldsymbol{u}$ is the momentum. $W = \gamma mc^2$ is the energy. $\gamma = (1-u^2)^{-1/2}$ refers to the relativistic formula factor, which is used for normalization. $\boldsymbol{u}$ is the speed normalized by the speed of c.

By observing Eqs. (11) and (12), both the laser electric field and the laser magnetic field in Subsection 2.1 affects the characteristics of the motion of the electron.[17] Meanwhile, Eqs. (11) and (12) are in the form of differential equations and are highly coupled. Considering the complexity of the equations, it is difficult to derive a general analytical solution. Combining Eqs. (1)–(6), differential equations are solved numerically using the Runge–Kutta–Fehlberg (RKF45) method. Then, we can obtain the trajectories, velocities, and accelerations of the electron. Since the higher order field effects are taken into account in Subsection 2.1, the numerical solution is more accurate.

2.3. Angular distribution of spatial radiation

When the electron does relativistic acceleration motion in the intense laser field, it emits electromagnetic radiation in all directions of space. To accurately calculate the angular distribution of the NTS radiation, the right-angle coordinate system in Fig. 1 is transformed into a spherical coordinate system. Defining the radiation direction vector $\boldsymbol{n} = (\sin\theta\cos\Phi, \sin\theta\sin\Phi, \cos\theta)$, Φ is the azimuthal angle and θ is the polar angle (marked in Fig. 2). The electromagnetic radiation power per unit solid angle can be expressed as[23]

$$\frac{\mathrm{d}P(t)}{\mathrm{d}\Omega} = \left[\frac{\left|\boldsymbol{n}\times\left[(\boldsymbol{n}-\boldsymbol{u})\times\left(\frac{\mathrm{d}\boldsymbol{u}}{\mathrm{d}t}\right)\right]\right|^2}{(1-\boldsymbol{n}\cdot\boldsymbol{u})^6}\right]_{t'}, \tag{13}$$

where $P(t)$ is radiation power and $\mathrm{d}P(t)/\mathrm{d}\Omega$ is normalized by $e^2\omega_0^2/(4\pi c)$. t' is the delay time of the electron. t is the moment when the observer receives the radiation. $t = t' + d_0 - \boldsymbol{n}\cdot\boldsymbol{D}$. Note that d_0 is the distance between the observation point of the detector and the point of action of the laser and the electron. $\boldsymbol{D}$ is the position vector of the electron.

The radiated energy per unit stereo angle of the electron can be considered as the accumulation of radiated power over a period of time. Hence, it can be expressed as the integral of the radiated power per unit stereo angle

$$\frac{\mathrm{d}W}{\mathrm{d}\Omega} = \int_{-\infty}^{+\infty} \frac{\left|\boldsymbol{n}\times\left[(\boldsymbol{n}-\boldsymbol{u})\times\left(\frac{\mathrm{d}\boldsymbol{u}}{\mathrm{d}t}\right)\right]\right|^2}{(1-\boldsymbol{n}\cdot\boldsymbol{u})^6}\mathrm{d}t. \tag{14}$$

3. Numerical results

In this paper, the radiation is observed on a sphere with a radius of 1 m centered at the origin of the coordinates. To eliminate the effects due to orders of magnitude, the radiated power of the electron is normalized (i.e., divided by the maximum radiated power of the electron in the spatial domain). As shown in Fig. 2, the color scale from blue to yellow indicates the radiated power of electron gradually increases. The brightest color (i.e., the yellowest place) indicates the maximum radiated power. The direction of the ray from the point of origin through this observation point is defined as the maximum radiation direction. In other words, the maximum radiation direction includes the azimuthal angle $\phi_{\max}$ and the polar angle $\theta_{\max}$.

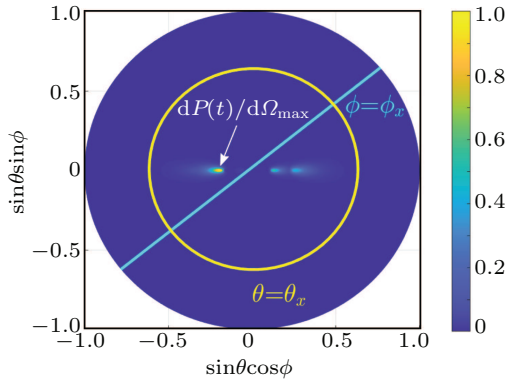


Fig. 2. Schematic diagram of the spatial spectrum of electron power radiation.

It should be noted that the laser wavelength $\lambda_0 = 1$ μm in this paper. In this section, the laser intensity I is characterized by the laser amplitude a_0 (see the beginning of Section 2 for the specific expression).

3.1. Laser intensity

According to the expression for the vector potential of a Gaussian laser pulse, the laser intensity is on the exponential term coefficient of the vector potential. Therefore, the increase in the laser intensity makes the vector potential change drastically. This drastic change directly affects the spatial radiation distribution of the electron.

3.1.1. Motion of the electron

As can be seen from Fig. 3, the motion of the electron under the action of a tightly focused linearly polarized laser consists of two main stages. In the first stage, the electron moves oscillating around the central axis of laser propagation, along the positive direction of the z-axis. The electron's velocity changes violently between two adjacent deflection points. Finally, the electron reaches the maximum radial distance from the central axis. In the second stage, after the electron experiences a violent acceleration, the rear of the laser is unable to decelerate the electron vertically to the previous situation. Therefore, the electron moves away from the central axis and gains energy.

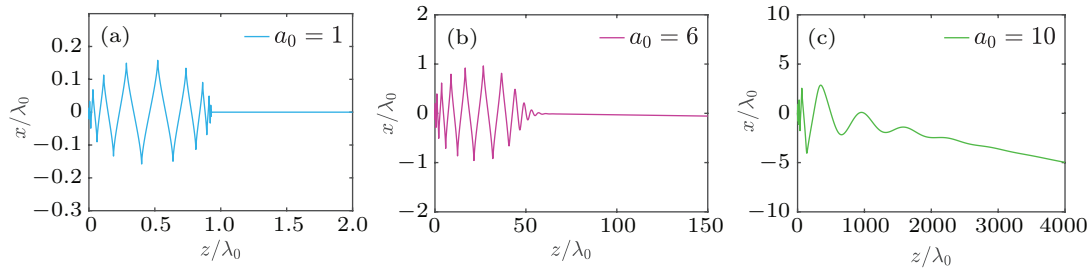


Fig. 3. Electron motion trajectories under the action of lasers of different laser intensities. The beam waist $w_0 = 3\lambda_0$, the pulse width $L = 3\lambda_0$, and the initial phase $\varphi_0 = 0$. The laser intensity is (a) $a_0 = 1$, (b) $a_0 = 6$, (c) $a_0 = 10$.

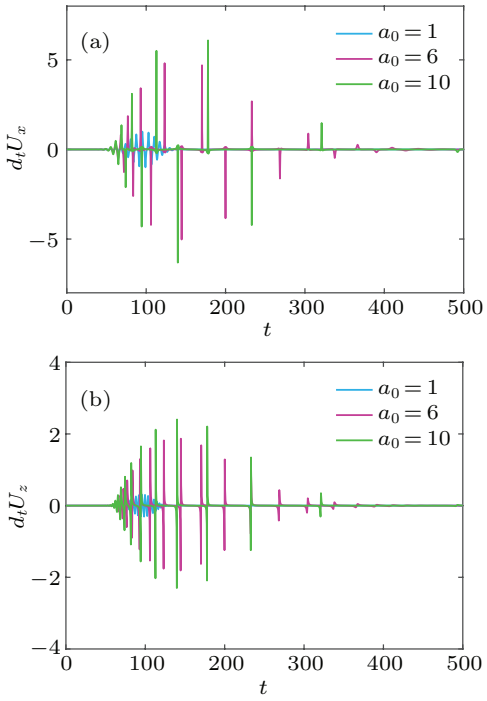


Fig. 4. Variation in acceleration of the electron under the action of lasers of different laser intensities. Beam waist radius $w_0 = 3\lambda_0$, pulse width $L = 3\lambda_0$, and the initial phase $\varphi_0 = 0$. (a) Variation in transverse acceleration $d_t U_x$, (b) variation in longitudinal acceleration $d_t U_z$.

The above two stages of motion are closely related to the intensity of the laser. When the laser intensity increases, the maximum radial distance reached by the electron is greater in the first stage. In the second stage, the off-axis motion of the electron becomes more pronounced. The specific reason can be explained based on the changes in the acceleration of the electron. As shown in Fig. 4, under the action of more intense laser pulse, the laser interacts with the electron for a longer period of time. The acceleration of the electron increases significantly. The electron is able to gain more energy. Meanwhile, the speed of the electron increases. This also explains the longer distance the electron oscillates in the first stage when the laser intensity increases (see Fig. 3).

In particular, when $a_0 > 6$, the acceleration of the electron changes extremely drastically, thus intensifying the oscillatory motion of the electron in the first stage. Moreover, the movement of the electron away from the central axis is more pronounced in the second stage. The characteristic of the electron motion leads to a change in the distribution of spatial radiation, i.e., the bifurcation phenomenon. This feature will be described in Subsection 3.1.2.

3.1.2. Spatial distribution of electron radiation

The Lorentz force generated by the laser magnetic field causes an enhanced longitudinal motion of the electron. The sharp change of longitudinal velocity causes the nonlinear characteristics of radiation. As depicted in Fig. 5, the increase in laser intensity leads to a smaller angular range of radiation. This phenomenon can be explained using the properties of electron motion in Subsection 3.1.1. The radiation produced by the electron is mainly concentrated in the direction of the motion.[8] Under the action of intense laser pulse, the

velocity of the electron motion is mainly in the longitudinal direction. When the laser intensity increases, the longitudinal motion of the electron is more pronounced. Therefore, the radiation angle of the electron is subsequently reduced. The phenomenon indirectly indicates the improvement of the collimation of the electron radiation, which is another main characteristic of electron nonlinear radiation.[19]

In Subsection 3.1.1, we mentioned that the acceleration of the electron changes extremely drastically when $a_0 > 6$. This drastic change leads to a bifurcation of the electron radiation in the space domain. In Fig. 5(b), when $a_0 = 6$, the electron radiation appears as two peaks in space. When $a_0 > 6$ the spatial distribution of electron radiation bifurcates, as shown in Fig. 5(c). The increase in laser intensity leads to a larger vector potential gradient. The velocity and acceleration of the electron at different positions vary considerably. As a result, radiation bifurcation occurs.

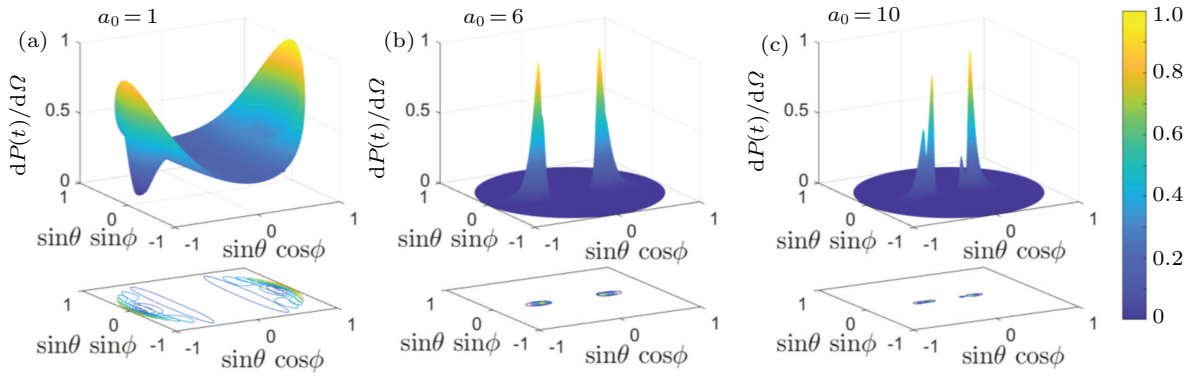


Fig. 5. Spatial distribution of electron radiation power under the action of lasers of different laser intensities. The beam waist $w_0 = 3\lambda_0$, the pulse width $L = 3\lambda_0$, and the initial phase $\varphi_0 = 0$. The laser intensity is (a) $a_0 = 1$, (b) $a_0 = 6$, (c) $a_0 = 10$.

3.1.3. Asymmetric radiation in the time domain

The dramatic changes in the electron acceleration lead to large differences in the radiated power from different angles. In this paper, the maximum value of the electron radiated power is defined as the peak power. We have defined the maximum radiation direction at the beginning of Section 3. As vividly shown in Fig. 6, in the direction of maximum radiation, a double peak appears on the curve of the radiated power per unit stereo angle versus time for the electron.

Lee *et al.* also found a double-peaked phenomenon of electron radiation in the time domain called the double-pulse structure.[27] In this paper, we refer to this phenomenon as the bimodal structure in the time domain for ease of understanding. In the following sections, the bimodal structure refers to the curve of the electron unit stereo angular radiation power versus time in the direction of maximum radiation. The bimodal structure in the time domain is a special phenomenon under the action of a linearly polarized laser. The appearance of the bimodal structure is mainly related to the longitudinal movement of the electron.[8,28] During half a period under the action of a linearly polarized laser (i.e., when the electron moves toward $\phi = \phi_{\max}$, $\theta = \theta_{\max}$), there exist zero points in the derivative of the longitudinal momentum of the electron with respect to time.[8,27] The acceleration of the electron produces peaks in radiated power for a brief period of time. The brief time is due to the delay time between the detector and the electron.[18,27] Therefore, the radiated power per unit stereo angle of the electron has two distinct peaks in the time domain.

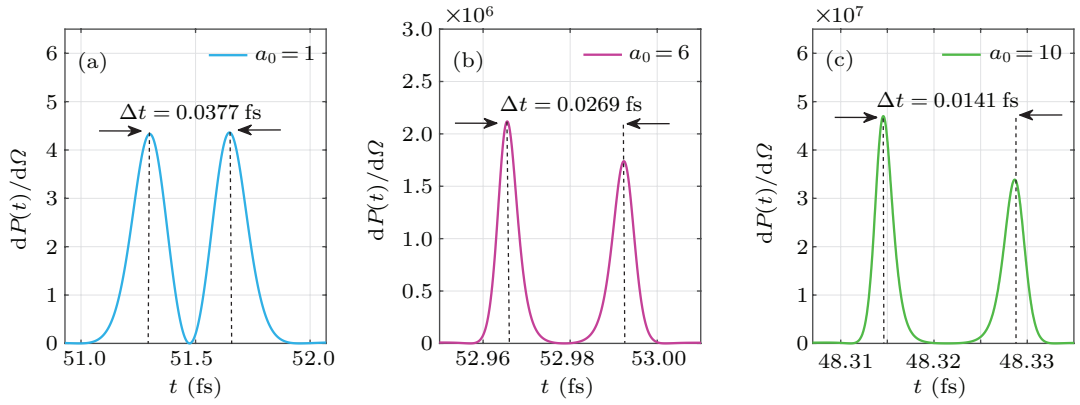


Fig. 6. In the direction of maximum radiation, the radiated power of the electron per unit stereo angle versus time. The beam waist $w_0 = 3\lambda_0$, the pulse width $L = 3\lambda_0$, and the initial phase $\varphi_0 = 0$. The laser intensity is (a) $a_0 = 1$, (b) $a_0 = 6$, (c) $a_0 = 10$.

However, compared to Lee's study, the bimodal structure we found is asymmetric. A tightly focused linearly polarized laser is different from a plane wave laser. The plane wave laser cannot achieve acceleration of the electron. Under the action of a plane wave laser, the acceleration and deceleration of the electron cancel each other out. Thus, the velocity of the electron is not increased. However, under the action of a tightly focused linearly polarized laser, the electron is able to maintain a certain speed and gain energy. Therefore, the bimodal structure we found is asymmetric under the action of a tightly focused linearly polarized laser.

As shown in Fig. 6, the bimodal structure in the time domain is significantly changed under the action of more intense laser pulses. In order to clearly compare the differences in the bimodal structure, we defined three parameters: the maximum radiated power $\mathrm{d}P(t)/\mathrm{d}\Omega_{\max}$, the symmetry coefficient S, and the bimodal interval Δt. $\mathrm{d}P(t)/\mathrm{d}\Omega_{\max}$ is the power at the highest peak. The symmetry coefficient S is to measure the symmetry of the bimodal structure defined as the ratio of the secondary peak to the primary peak. Its range is (0,1). The closer the symmetry coefficient S is to 1, the better the symmetry of the bimodal structure is. Δt is the difference between the moment of peak appearance $t_{\max}$ and the moment of secondary peak appearance $t_{\mathrm{s_max}}$, $\Delta t = |t_{\max} - t_{\mathrm{s_max}}|$.

Table 1. Parameters of the bimodal structure in lasers of different laser intensities.

a_0	$\mathrm{d}P(t)/\mathrm{d}\Omega_{\max}$	S	Δt (fs)
1	4.3612	0.9929	0.0377
6	2.12×10^{6}	0.8208	0.0269
10	4.70×10^{7}	0.7204	0.0141

The specific data for the above parameters in Fig. 6 are shown in Table 1. The peak of electron radiation power increases under the action of more intense laser pulses. According to Eq. (13), it can be found that the radiated power of the electron is related to the acceleration of the electron. The higher the intensity of the laser, the greater the acceleration of the electron, and the consequent increase in the peak power of the radiation. However, under the action of more intense laser pulse, the symmetry of the electron radiation decreases significantly, and the bimodal interval becomes smaller. Note that the increase in laser intensity is unable to increase the maximum radiated power as well as the symmetry of the bimodal structure at the same time.

As for the higher intensity laser pulses, they will be specifically analyzed in the next section in combination with the initial phase.

3.2. Initial phase

In practice, the intensity of the laser is often limited in order to ensure the safety of the experiment. Within the limited laser parameters, the initial phase can be adjusted to obtain a larger radiated power. When the pulse width (i.e., half height full width) of the intense laser is larger, the number of electron oscillations increases. As a result, the effect of the initial phase on the electron radiation is masked.[29] In this section, the pulse width of the laser is $3\lambda_0$, and the effect of the initial phase is well represented. It is important to note that the initial phase of the laser in this section varies from 0 to 2π with an interval of $\pi/18$.

3.2.1. Periodic extension

Based on Subsection 3.1.1, the motion of the electron mainly consists of two stages. The initial phase can change the maximum radial distance reached by the electron in the first stage. In the second stage, the initial phase is able to change the direction of the electron away from the central axis. As vividly depicted in Fig. 7, when the laser intensity is fixed (e.g., $a_0 = 25$), the motion trajectory of the electron obeys a periodic variation with a period of 2π. When the initial phase difference is π, the trajectory of the electron is symmetric about the propagation central axis. In other words, when the initial phase increases by π, the electron has equal maximum radial distance in the first stage. In the second stage, the electron flips once in the direction away from the central axis. When the initial phase is changed by 2π, the trajectories of the electron almost overlap.

As can be seen from Fig. 8, it can be concluded that the spatial radiation of the electron is mainly concentrated in the plane of polarization (XOZ plane). It also indicates that the azimuth angle $\Phi_{\max}$ can only take the value of 0 or π. In Fig. 9, we plotted the variation in azimuthal angle $\Phi_{\max}$ and polar angle $\theta_{\max}$ under the action of lasers with different initial phases. The azimuth angle $\Phi_{\max}$ is flipped once when the initial phase changes by π. Interestingly, when the initial phase changes by π, the electron changes once in the direction away from the central axis in the second stage (as mentioned above). If the azimuthal angle $\Phi_{\max} = 0$, it means that the maximum radiated power is generated when the velocity of the electron in the x-direction (i.e., u_x) is positive. If the azimuthal angle $\Phi_{\max} = \pi$, it means that the maximum radiated power is generated when the velocity of the electron in the x-direction (i.e., u_x) is negative. Therefore, the maximum radiation direction is closely related to the trajectory of the electron. In addition, it can be found that the polar angle $\theta_{\max}$ shows a periodic variation with a period of π. Within a period (marked in Fig. 9), the polar angle $\theta_{\max}$ shows an overall increasing trend. Considering that the polar angle $\theta_{\max}$ is less than $\pi/2$, the radiation of the electron is forward radiation.

Based on the azimuthal angle $\Phi_{\max}$ and polar angle $\theta_{\max}$ shown in Fig. 9, the maximum radiation direction can be deter-

mined. Therefore, we plotted the curve of the radiated power per unit stereo angle of the electron with time in the direction of maximum radiation, as shown in Fig. 10. It can be found that there is also a periodic variation in the bimodal structure in the time domain. Due to the large number of selected initial phases, it is not possible to describe each bimodal structure by amplification. Therefore, we still describe the bimodal structure with the parameters in Subsection 3.1.3, i.e., the maximum radiated power $\mathrm{d}P(t)/\mathrm{d}\Omega_{\max}$, the symmetry coefficient S, and the bimodal interval Δt.

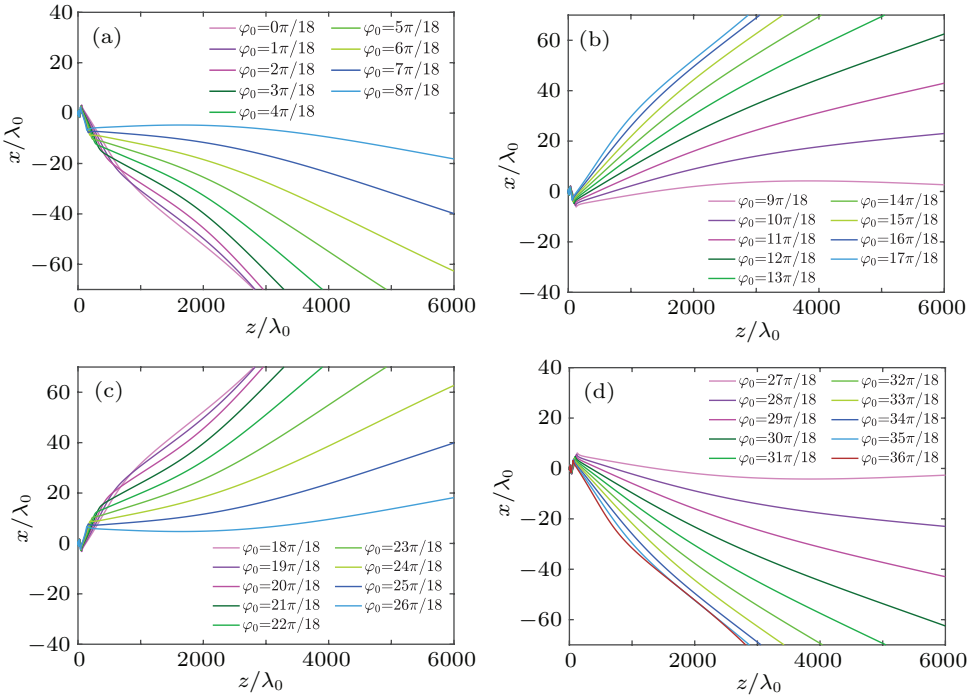


Fig. 7. The trajectories of the electron under the action of lasers with different initial phases. The beam waist $w_0 = 3\lambda_0$, the pulse width $L = 3\lambda_0$, and the laser intensity $a_0 = 25$. The range of the variation in the initial phase φ_0 is (a) 0–$8\pi/18$, (b) $9\pi/18$–$17\pi/18$, (c) $18\pi/18$–$26\pi/18$, (d) $27\pi/18$–$36\pi/18$.

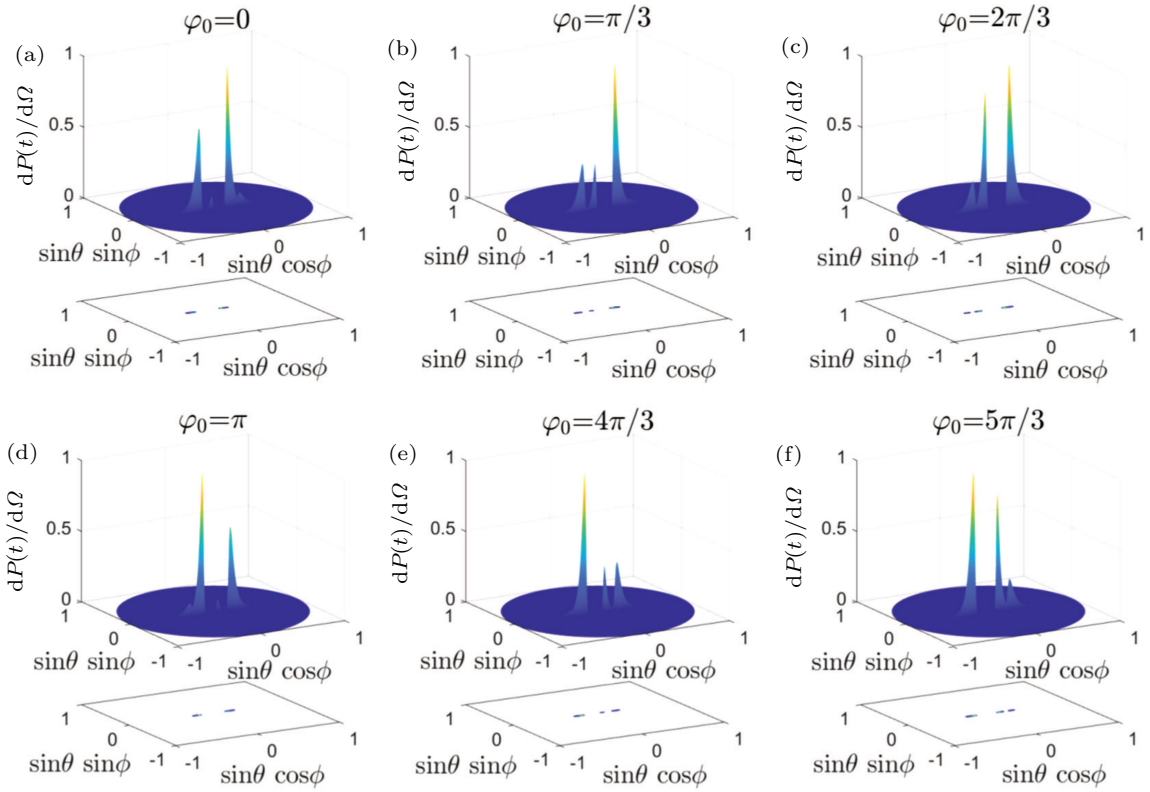


Fig. 8. Spatial distribution of electron radiation power under the action of lasers with different initial phases. The beam waist $w_0 = 3\lambda_0$, the pulse width $L = 3\lambda_0$, and the laser intensity $a_0 = 25$. The initial phase is (a) $\varphi_0 = 0$, (b) $\varphi_0 = \pi/3$, (c) $\varphi_0 = 2\pi/3$, (d) $\varphi_0 = \pi$, (e) $\varphi_0 = 4\pi/3$, (f) $\varphi_0 = 5\pi/3$.

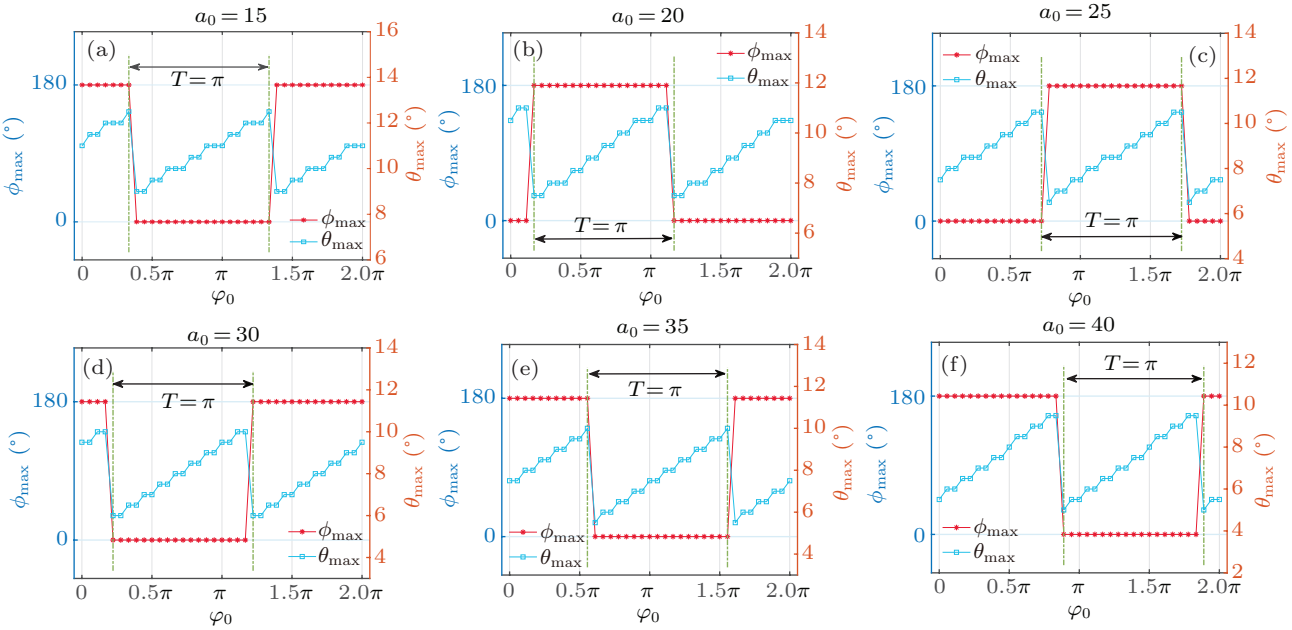


Fig. 9. Variation in the radiation azimuth angle $\Phi_{\max}$ and polar angle $\theta_{\max}$ under the action of lasers with different initial phases. The beam waist $w_0 = 3\lambda_0$, and the pulse width $L = 3\lambda_0$. The laser intensity is (a) $a_0 = 15$, (b) $a_0 = 20$, (c) $a_0 = 25$, (d) $a_0 = 30$, (e) $a_0 = 35$, (f) $a_0 = 40$.

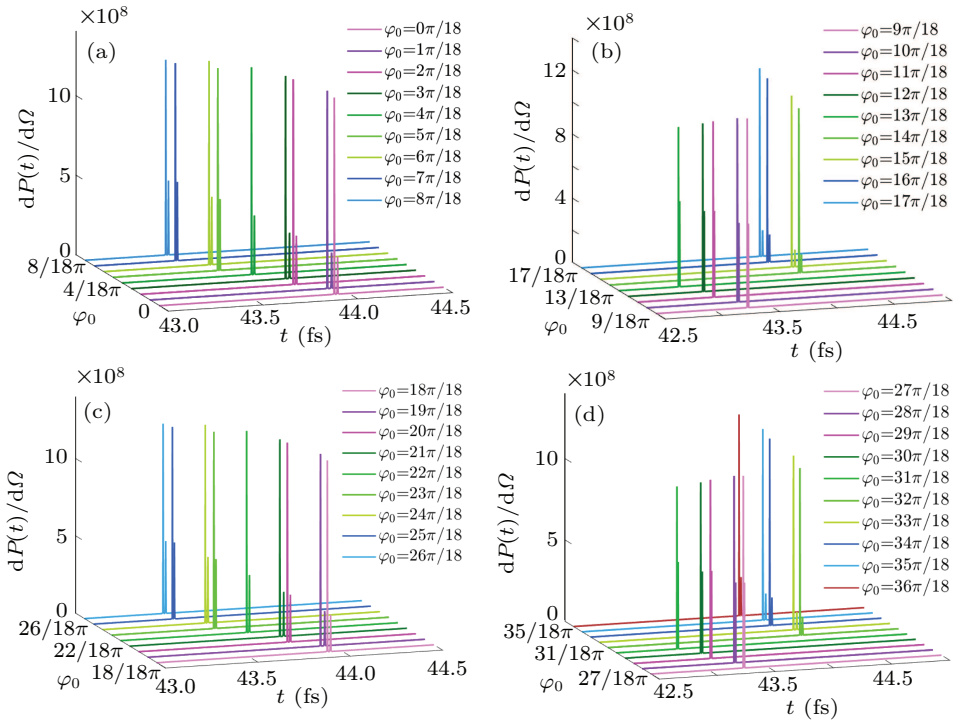


Fig. 10. In the direction of maximum radiation, the radiated power of the electron per unit stereo angle versus time. The beam waist $w_0 = 3\lambda_0$, the pulse width $L = 3\lambda_0$, and the laser intensity $a_0 = 25$. The range of variation in the initial phase φ_0 is (a) 0–$8\pi/18$, (b) $9\pi/18$–$17\pi/18$, (c) $18\pi/18$–$26\pi/18$, (d) $27\pi/18$–$36\pi/18$.

As shown in Fig. 11, the maximum radiated power $\mathrm{d}P(t)/\mathrm{d}\Omega_{\max}$ shows a periodic variation. Interestingly, the variation period of $\mathrm{d}P(t)/\mathrm{d}\Omega_{\max}$ is π, which is half of the period of the electron motion trajectory. According to Eq. (13), it can be found that the radiated power of the electron is non-negative. Given the above analysis, it can be determined that the trajectory of the electron is symmetric about the central axis when the initial phase differs by π. In other words, the maximum radial distance is the same, while the direction away from the central axis is different. Therefore, the radiated power per unit stereo angle of the electron is the same when the initial phase differs by π. The only difference is whether the velocity of the electron in the x direction (i.e., u_x) is positive or negative when the maximum radiated power is generated. This is why the maximum radiated power $\mathrm{d}P(t)/\mathrm{d}\Omega_{\max}$ shows a periodic extension with a period of π.

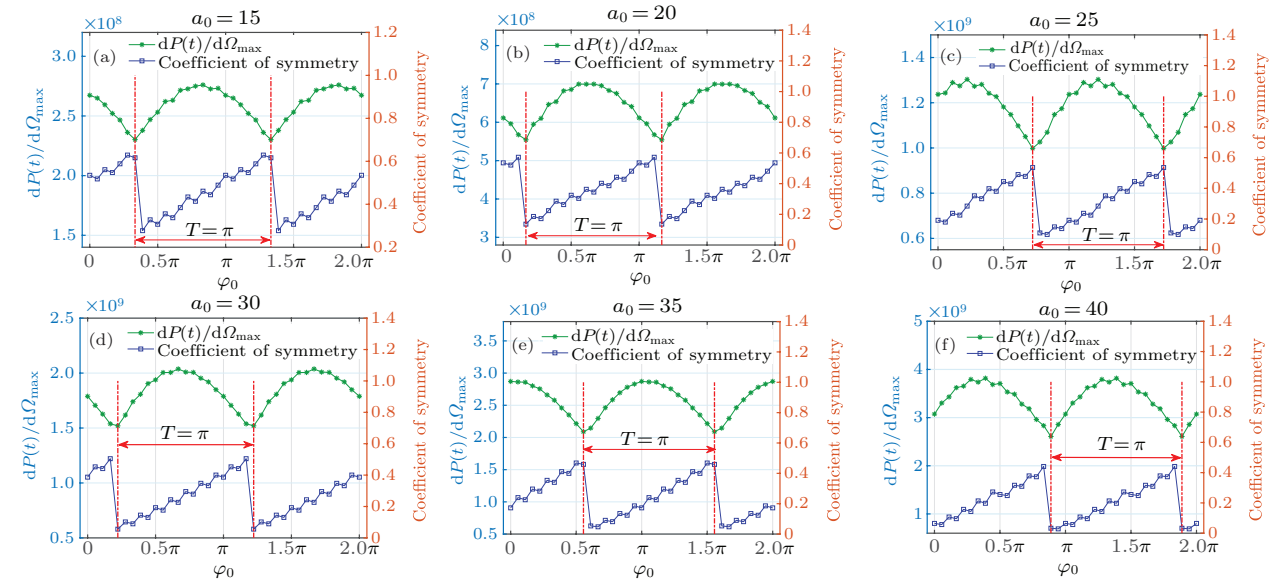


Fig. 11. The variation in the maximum radiated power $\mathrm{d}P(t)/\mathrm{d}\Omega_{\max}$ and the symmetry coefficient S under the action of lasers with different initial phases. The beam waist $w_0 = 3\lambda_0$, and the pulse width $L = 3\lambda_0$. The laser intensity is (a) $a_0 = 15$, (b) $a_0 = 20$, (c) $a_0 = 25$, (d) $a_0 = 30$, (e) $a_0 = 35$, (f) $a_0 = 40$.

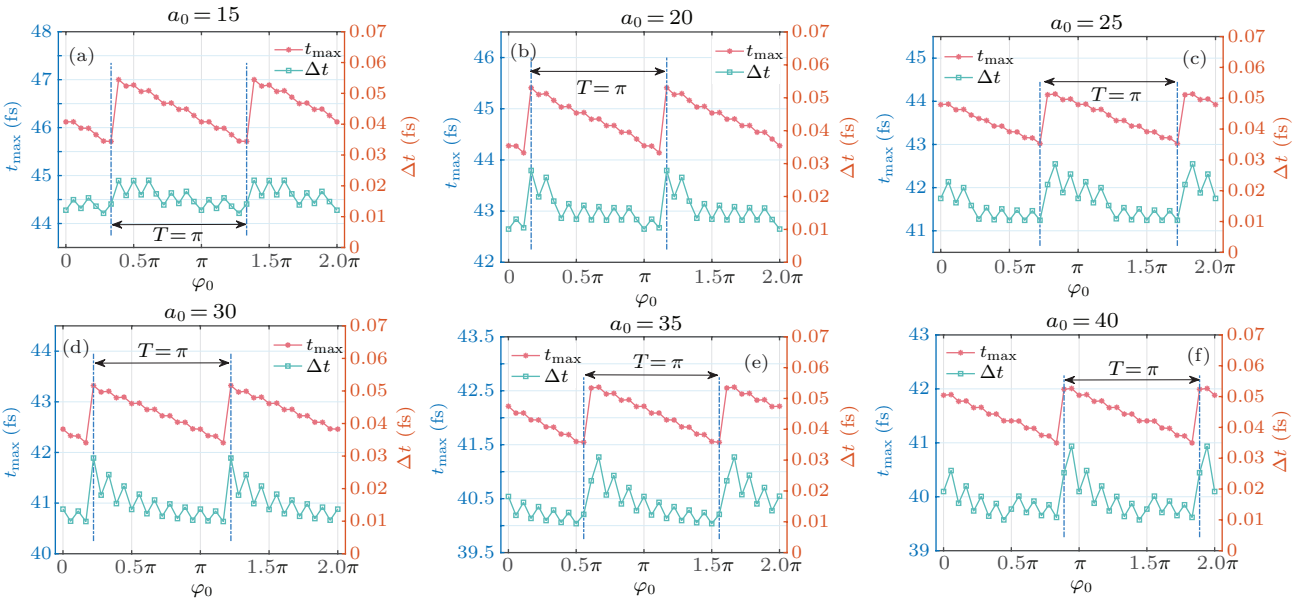


Fig. 12. The variation in the bimodal interval Δt and the moment of peak appearance $t_{\max}$ under the action of lasers with different initial phases. The beam waist $w_0 = 3\lambda_0$, and the pulse width $L = 3\lambda_0$. The laser intensity is (a) $a_0 = 15$, (b) $a_0 = 20$, (c) $a_0 = 25$, (d) $a_0 = 30$, (e) $a_0 = 35$, (f) $a_0 = 40$.

Combining Figs. 11 and 12, it is found that the symmetry coefficient S, the bimodal interval Δt, and the moment of peak appearance $t_{\max}$ also show periodic variations with a period of π. However, the changes of S, Δt and $t_{\max}$ are discontinuous. There are large jumps in S, Δt and $t_{\max}$ at the articulation of some phases. In contrast, the maximum radiated power of electron $\mathrm{d}P(t)/\mathrm{d}\Omega_{\max}$ is more continuous. The specific cycle intervals have been labeled in Figs. 11 and 12. The specific reasons for the jump will be described in Subsection 3.2.2.

In one cycle, the maximum radiated power of the electron $\mathrm{d}P(t)/\mathrm{d}\Omega_{\max}$ increases and then decreases. The maximum value of $\mathrm{d}P(t)/\mathrm{d}\Omega_{\max}$ is obtained in the middle of a cycle. The symmetry of the bimodal structure shows an overall increasing trend within one cycle. In addition, the peak appearance moment $t_{\max}$ and the bimodal interval Δt show an overall decreasing trend within one cycle. Therefore, within the limited laser intensity, the maximum radiated power, or the bimodal structure with better symmetry, can be obtained by adjusting the initial phase.

3.2.2. Jumping point

In Subsection 3.2.1, the symmetry coefficient S, the peak appearance moment $t_{\max}$ and the bimodal interval Δt show significant changes at some initial phases. Taking $a_0 = 25$ as an example, it can be found that S, Δt, and $t_{\max}$ all change significantly at the same phase. This phase is called the jump point. As the initial phase varies from 0 to 2π, the asymmetric

radiation of the electron undergoes two jump points. For example, when $a_0 = 25$, the jump points are $\varphi_0 = 134\pi/180$ and $314\pi/180$ (determined by numerical simulations with higher accuracy).

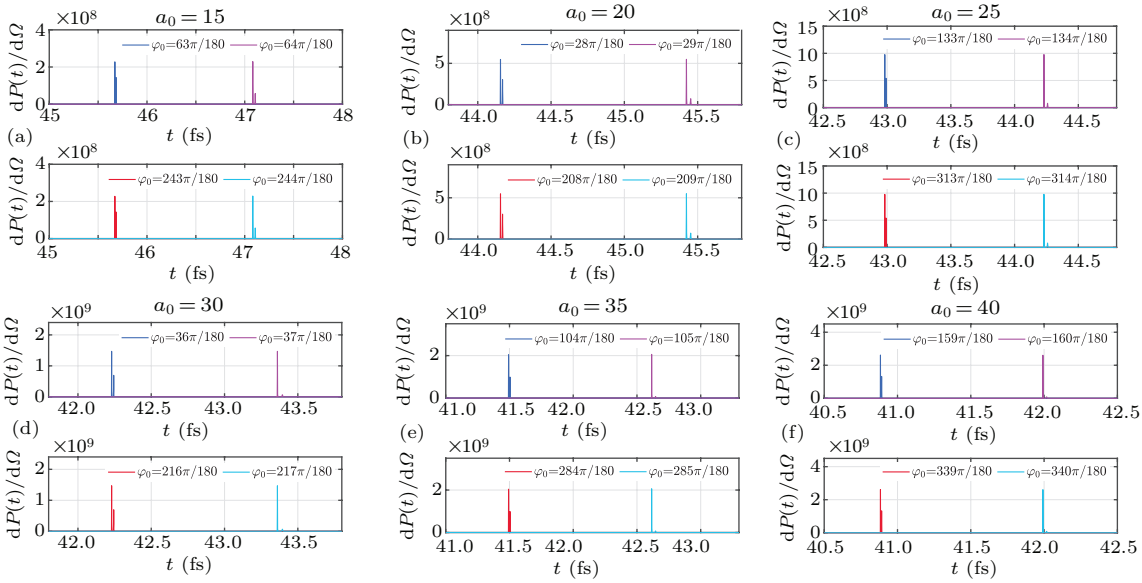


Fig. 13. In the maximum radiation direction, the bimodal structure in the time domain before and after the jump point. The beam waist $w_0 = 3\lambda_0$, and the pulse width $L = 3\lambda_0$. The laser intensity is (a) $a_0 = 15$, (b) $a_0 = 20$, (c) $a_0 = 25$, (d) $a_0 = 30$, (e) $a_0 = 35$, (f) $a_0 = 40$.

Combined with Figs. 9–12, the phenomenon of the jump point can be explained. The jump point arises due to the jump in the direction of maximum radiation, i.e., the jump in the azimuthal angle $\Phi_{\max}$. To be more precise, the change in velocity of the electron in the x-direction (i.e., u_x) leads to the jump point. In Subsection 3.2.1, we pointed out the specific relationship between the azimuthal angle $\Phi_{\max}$ and u_x. Taking $a_0 = 25$ as an example, the maximum radiated power of the electron at $\varphi_0 = 133\pi/180$ is generated by u_x being positive. The variation in the initial phase causes a change in the electron velocity.[29,30] When $\varphi_0 = 134\pi/180$, the maximum radiated power of the electron when u_x is negative exceeds that when u_x is positive. Therefore, the maximum radiation direction then makes a jump. Meanwhile, the asymmetric radiation of the electron also undergoes a large change, i.e., a jump in the bimodal structure (see Figs. 10(b) and 10(d)). The maximum radiated power $dP(t)/d\Omega_{\max}$ is not directly related to the direction of u_x, so it is continuous.

As shown in Fig. 13, the bimodal structure is plotted before and after the jump point in the direction of maximum radiation. It can be clearly seen that after the jump point, the bimodal structure of the electron has a worse symmetry. This phenomenon is consistent with the findings in Fig. 11. Interestingly, the distance between the two jump points differs by π in the range of 0–2π. This distance is equal to the period of change of the electron asymmetric radiation.

Note that after extensive numerical simulations, it was found that there is always a jump point in the asymmetric radiation of the electron, regardless of the laser intensity. In other words, the jump point is the necessary point for the effect of the initial phase on the asymmetric radiation of the electron.

3.3. Effect of laser intensity on electron asymmetric radiation considering the initial phase

In Subsection 3.2, it can be found that the maximum radiated power or a bimodal structure with optimal symmetry can be obtained by adjusting the initial phase within a finite laser intensity. In particular, the effect of the initial phase cannot be neglected under the action of an intense laser with short pulse width ($a_0 \geq 15$, $L = 3\lambda_0$). Based on the conclusions in Subsection 3.2.1, the effect of laser intensity on electron asymmetric radiation is discussed specifically, in particular, the variation in the bimodal structure.

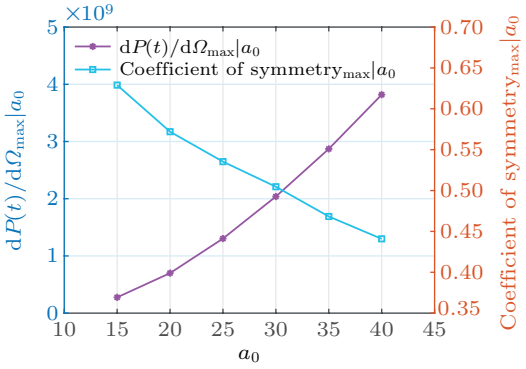


Fig. 14. The maximum radiated power and the maximum coefficient of symmetry that can be obtained by adjusting the initial phase under the action of lasers with different laser intensities. The beam waist $w_0 = 3\lambda_0$, and the pulse width $L = 3\lambda_0$.

It should be declared that $dP(t)/d\Omega_{\max}|a_0$ is the maximum radiated power that can be obtained by adjusting the initial phase within a finite laser intensity. Intuitively,

$\mathrm{d}P(t)/\mathrm{d}\Omega_{\max}|a_0$ is the maximum value of $\mathrm{d}P(t)/\mathrm{d}\Omega_{\max}$ as shown in Fig. 11. Similarly, coefficient of symmetry$_{\max}|a_0$ is the maximum symmetry coefficient that can be obtained by adjusting the initial phase within a finite laser intensity, i.e., the maximum value of coefficient of symmetry shown in Fig. 11.

As shown in Fig. 14, the maximum radiated power that can be achieved under the action of a more intense laser increases. However, the symmetry of the bimodal structure decreases significantly. This conclusion is in agreement with the one in Subsection 3.1.3.

3.4. Pulse width

It is emphasized again that the pulse width in this paper is half height full width. Based on Eq. (7), the pulse width of the laser affects the electromagnetic field component of the laser, which in turn affects the motion characteristics of the electron. The maximum acceleration of the electron is defined as the maximum amplitude of the change in acceleration. It can be observed from Fig. 15 that the maximum acceleration decreases as the laser pulse increases. Under the action of the short-pulse laser, the acceleration of the electron is greater, and the time required for the electron to accelerate to the speed of light is shorter.

The increase in pulse width causes a more intensive and violent acceleration change. This change leads to a significant change in the spatial domain of the electron radiation. Under the action of a short-pulse laser, the number of electron accelerations is limited, and thus the radiation range of the electron is smaller. When the pulse width increases, the violent acceleration changes cause the coupling of electron radiation, which increases the radiation range (see Fig. 16).

Similarly, we plotted the asymmetric bimodal structure under the action of lasers of different pulse widths. As depicted in Fig. 17, the maximum radiated power of electron $\mathrm{d}P(t)/\mathrm{d}\Omega_{\max}$ decreases as the pulse width of the laser increases. From the perspective of electron dynamics, the decrease in the maximum acceleration leads to a decrease in the electron radiated power. Meanwhile, the moment of peak appearance $t_{\max}$ becomes longer. This phenomenon is caused, on the one hand, by the increase in the number of radiated attosecond pulses.[8] On the other hand, it is affected by the decrease in the maximum acceleration of the electron.

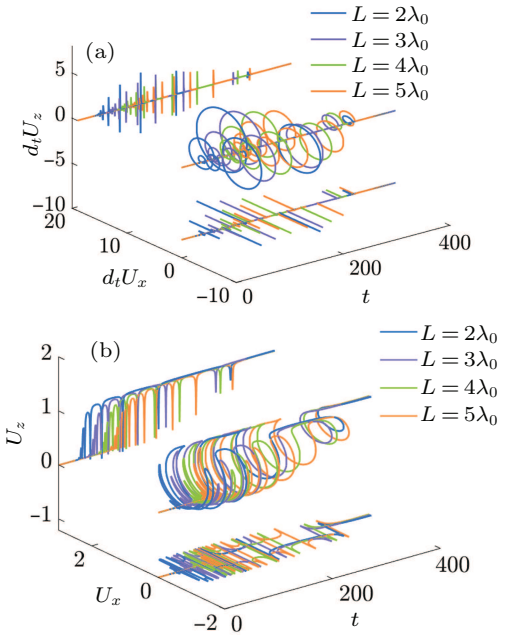


Fig. 15. Variation in the velocity and acceleration of the electron under the action of lasers of different pulse widths. The laser intensity $a_0 = 15$, the beam waist $w_0 = 3\lambda_0$, and the initial phase $\varphi_0 = 0$. (a) Variation in total acceleration and its longitudinal and transverse acceleration. (b) Variation in total velocity and its longitudinal and transverse velocity.

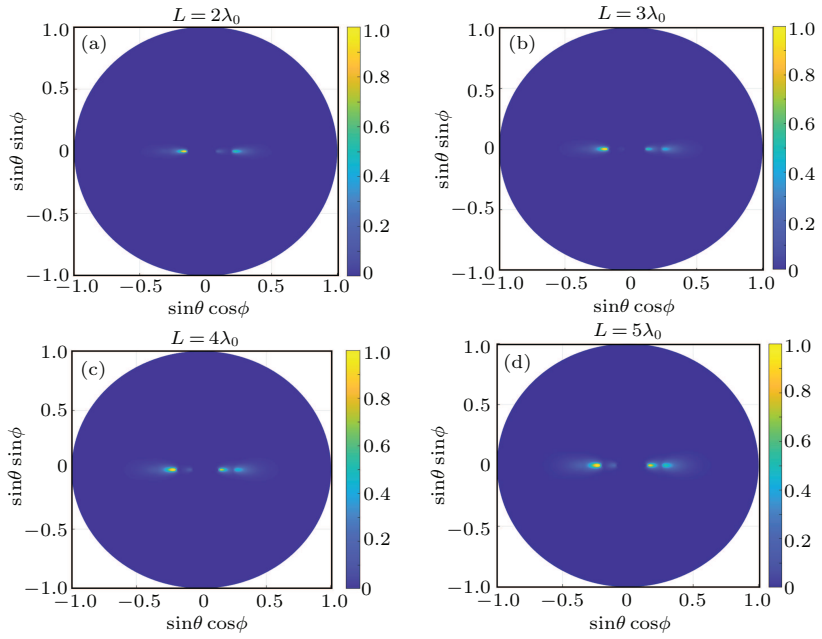


Fig. 16. Spatial distribution of electron radiation power under the action of lasers of different pulse widths. The laser intensity $a_0 = 15$, the beam waist $w_0 = 3\lambda_0$, and the initial phase $\varphi_0 = 0$. The pulse width is (a) $L = 2\lambda_0$, (b) $L = 3\lambda_0$, (c) $L = 4\lambda_0$, (d) $L = 5\lambda_0$.

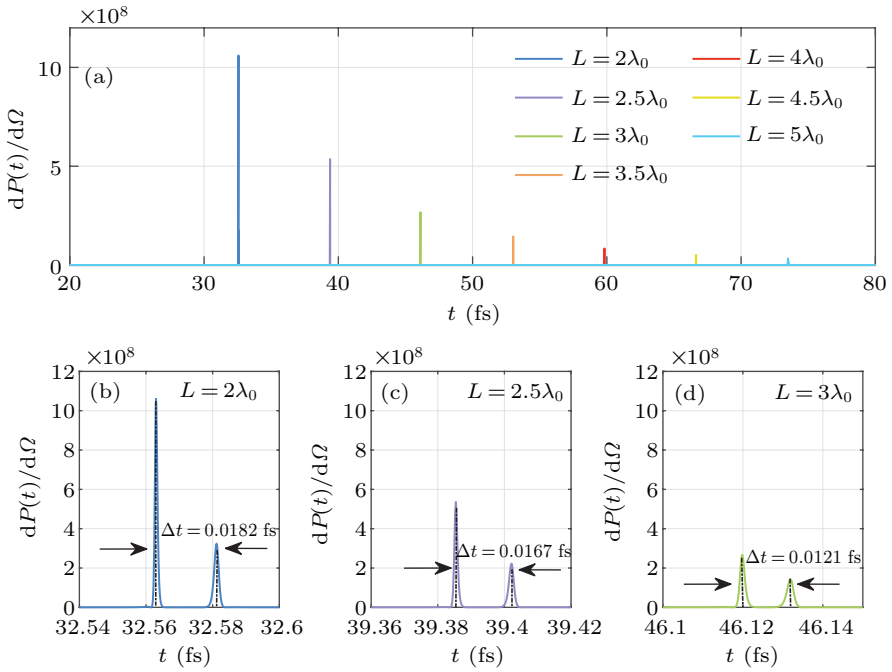


Fig. 17. In the direction of maximum radiation, the radiated power of the electron per unit stereo angle versus time. The laser intensity $a_0 = 15$, the beam waist $w_0 = 3\lambda_0$, and the initial phase $\varphi_0 = 0$. (a) Overall comparison diagram. (b)–(d) Enlarged plots of some curves in (a). The pulse width is (b) $L = 2\lambda_0$, (c) $L = 2.5\lambda_0$, (d) $L = 3\lambda_0$.

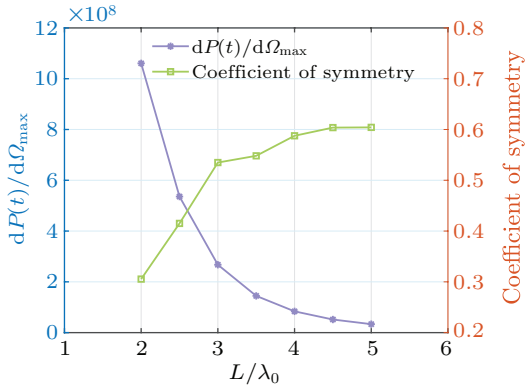


Fig. 18. The variation in the maximum radiated power $\mathrm{d}P(t)/\mathrm{d}\Omega_{\max}$ and the symmetry coefficient S under the action of laser with different pulse widths. The laser intensity $a_0 = 15$, the beam waist $w_0 = 3\lambda_0$, and the initial phase $\varphi_0 = 0$.

As the pulse width of the laser increases, the maximum radiated power of the electron decreases. However, the asymmetry of electron radiation is well mitigated. As shown in Fig. 18, when the pulse width of the laser is small (e.g., $L \leq 3\lambda_0$), there are drastic changes in the maximum radiated power and symmetry coefficient of the electron. When the pulse width of the laser is larger, the variation in both is smaller and stabilizes.

3.5. Radiation spectrum

In addition, we investigated the effect of laser parameters on the electron radiation spectrum to deepen the understanding of nonlinear Thomson scattering. As shown in Fig. 19, under the action of intense laser pulses, the electronic harmonic radiation energy oscillates decreasingly as the harmonic radiation frequency increases, and finally tends to stabilize. In other words, there appear multiple peaks and near-zero valleys in the electronic harmonic radiated energy. When the laser intensity increases or the pulse width decreases, the maximum energy of the electronic harmonic radiation is increased. Meanwhile, the redshift phenomenon in the frequency domain is present.[31] Based on the properties of the spectrum, it can be inferred that the electron produces coherent radiation.[18,28,32]

Interestingly, there is also a periodic variation in the maximum energy of the electronic harmonic radiation with a period of π when the initial phase varies (see Fig. 20).

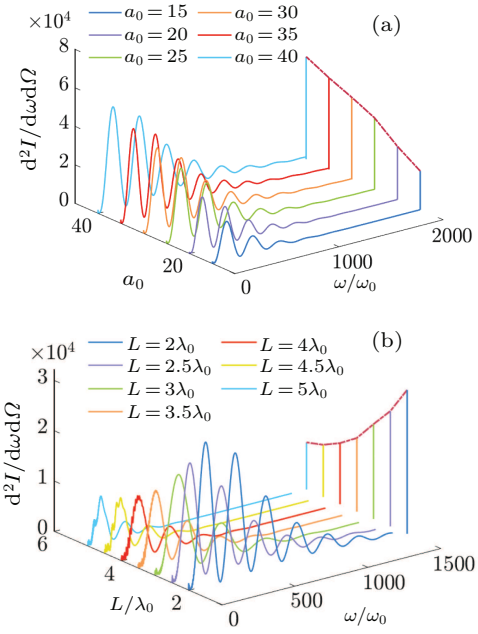


Fig. 19. (a) Spectrum in the direction of maximum radiation under the action of lasers with different laser intensities. (b) Spectrum in the direction of maximum radiation under the action of lasers with different pulse widths. The laser intensity $a_0 = 15$, and the beam waist $w_0 = 3\lambda_0$.

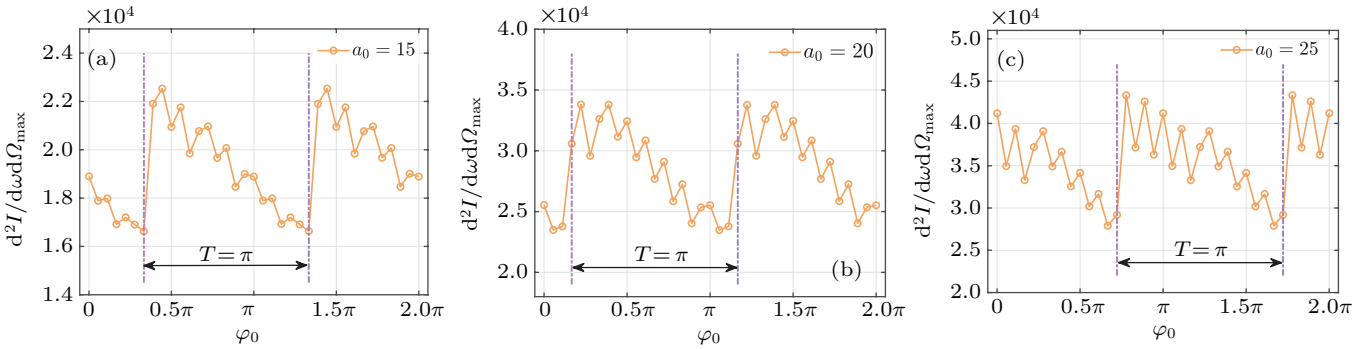


Fig. 20. Variation in the maximum energy of the electron harmonic radiation under the action of lasers with different initial phases. The beam waist $w_0 = 3\lambda_0$, and the pulse width $L = 3\lambda_0$. The laser intensity is (a) $a_0 = 15$, (b) $a_0 = 20$, (c) $a_0 = 25$.

4. Conclusion and perspectives

Under the framework of the single-electron model, the influence of laser parameters on the electron nonlinear radiation is systematically studied. In the direction of maximum radiation, a bimodal structure exists in the time domain. The increase of laser intensity, while significantly increasing the electron radiation power, intensifies the asymmetry of electron radiation. Especially when $a_0 > 6$, the oscillatory motion of electron is more violent, which causes the spatial distribution of electron radiation to bifurcate. Based on the view of electron dynamics, an explanation for the asymmetric bimodal structure is given. The variation in the initial phase leads to a periodic variation in the electron motion with a period of 2π. Considering the non-negativity of the electron radiated power, the maximum radiated power of the electron and its observed direction vary periodically with a period of π. The existence of jump points with a phase difference of π in the range of 0–2π is found. Moreover, the increase in pulse width reduces the radiation power, expands the radiation range, and alleviates the asymmetry of the radiation. In the frequency domain, the variation in the electron harmonic radiated energy is analyzed to enhance the understanding of the NTS. The findings of this paper contribute to the understanding and application of the nonlinear radiation of the electron in intense lasers. Based on the above conclusions, by adjusting the laser intensity, initial phase, and pulse width, a radiation source with higher power and better symmetry can be obtained.

Acknowledgements

Project supported by the National Natural Science Foundation of China (Grant Nos. 10947170/A05 and 11104291), Natural Science Fund for Colleges and Universities in Jiangsu Province (Grant No. 10KJB140006), Natural Science Foundation of Shanghai (Grant No. 11ZR1441300), and Natural Science Foundation of Nanjing University of Posts and Telecommunications (Grant No. NY221098), and sponsored by the Jiangsu Qing Lan Project and STITP Project (Grant No. CXXYB2022516).

References

[1] Hartemann F V and Kerman A K 1996 *Phys. Rev. Lett.* **76** 624
[2] Strickland D and Mourou G 1985 *Opt. Commun.* **55** 447
[3] Witte S, Zinkstok R Th, Hogervorst W and Eikema K S E 2005 *Opt. Express* **13** 4903
[4] Maine P, Strickland D, Bado P, Pessot M and Mourou G 1988 *IEEE J. Quantum Electron.* **24** 398
[5] Liu C P, Markus C K, Karen Z H, Carsten M and Christoph H K 2009 *New J. Phys.* **11** 105045
[6] Rykovanov S G, Geddes C G R, Schroeder C G, Esarey E and Leemans W P 2016 *Phys. Rev. Accel. Beams* **19** 030701
[7] Zheng Y L, Cai X M, Zhao X and Wang W 2022 *Opt. Express* **30** 1627
[8] Zheng J, Sheng Z M, Zhang J, Wei Z Y and Yu W 2005 *Acta Phys. Sin.* **54** 1018 (in Chinese)
[9] Suortti P and Thomlinson W 2003 *Phys. Med. Biol.* **48** R1
[10] Chi Z, Du Y, Huang W and Tang C 2020 *J. Synchrotron Rad.* **27** 737
[11] Baltuška A, Udem Th, Uiberacker M, Hentschel M, Goulielmakis E, Gohle C, Holzwarth R, Yakovlev V S, Scrinzi A, Hänsch T W and Krausz F 2003 *Nature* **421** 593
[12] Kunwar Pal S, Rashmi A and Anil K M 2015 *J. Apply. Phys.* **118** 104902
[13] Huang H S and Deng H X 2021 *Optica* **8** 1020
[14] Zhang K J, Liu L, Zeng Q W, Gao T C, Hu S and Chen M 2019 *Acta Phys. Sin.* **68** 194207 (in Chinese)
[15] Krajewska K, Twardy M and Kamínski J Z 2014 *Phys. Rev. A* **89** 052123
[16] Szabolcs H, Sándor V and Attila C 2018 *New J. Phys.* **20** 073043
[17] Wang Y B, Yang Q Y and Tian Y W 2023 *Laser Phys. Lett.* **20** 035401
[18] Lee K, Kim B H and Kim D 2005 *Phys. Plasmas* **12** 043107
[19] Chang Y F, Zeng Z R, Wang C, Long Z N and Tian Y W 2022 *Appl. Opt.* **61** 6038
[20] Alexandru Popa 2008 *J. Phys. B: At. Mol. Opt. Phys.* **41** 015601
[21] Hartemann F V, Troha A L, Luhmann N C Jr and Toffano Z 1996 *Phys. Rev. E* **54** 2956
[22] Cao W, Lan P F and Lu P X 2006 *Acta Phys. Sin.* **55** 2115 (in Chinese)
[23] Lü C Y, Chen Z Y, Zhu W X and Tian Y W 2022 *Laser Technology* **46** 422
[24] Salamin Y I, Mocken G R and Keitel C H 2002 *Phys. Rev. Spec. Top.-Ac.* **5** 101301
[25] Li J X, Zang W P and Tian J G 2010 *Appl. Phys. Lett.* **96** 031103
[26] Salamin Y I and Keitel C H 2002 *Phys. Rev. Lett.* **88** 095005
[27] Lee K, Cha Y H, Shin M S, Kim B H and Kim D 2003 *Phys. Rev. E* **67** 026502
[28] Vais O E, Bochkarev S G and Bychenkov V Y 2016 *Plasma Phys. Rep.* **42** 818
[29] Lan P F, Lu P X and Cao W 2007 *Acta Phys. Sin.* **56** 2482 (in Chinese)
[30] He X K, Li R X, Shuai B, Ge X C and Xu Z Z 2005 *Phys. Plasmas* **12** 073101
[31] Chang Y F, Wang C, Wang Y B, Long Z N, Zeng Z R and Tian Y W 2022 *Laser Phys. Lett.* **19** 065301
[32] Mohammad Vaziri, Mojtaba Golshani, Sozha Sohaily and Alireza Bahrampour 2015 *Phys. Plasmas* **22** 033118